Computer-aided Design and Manufacturing of a Patented, Left Ventricle Assist Device Positioning Tool – 3D Navigated Surgical Treatment of End-Stage Heart Failure

Imre Janos Barabas

Heart and Vascular Center, 3D Center, Semmelweis University
Városmajor u. 68, 1122 Budapest, Hungary
barabas.janos_imre@med.semmelweis-univ.hu

Bela Merkely, Istvan Hartyanszky

Heart and Vascular Center, Semmelweis University
Városmajor u. 68, 1122 Budapest, Hungary
rektor@semmelweis-univ.hu; hartyanszky.istvan@med.semmelweis-univ.hu

Daniel Palkovics

3D Center, Semmelweis University, Városmajor u. 68, 1122 Budapest, Hungary
Department of Periodontology, Semmelweis University, Szentkirályi u. 47, 1088 Budapest, Hungary
palkovics.daniel@dent.semmelweis-univ.hu

Abstract: The Left Ventricular Assist Device (LVAD), is a leading therapy option for patients with end-stage heart failure. A successful LVAD implantation is influenced by various factors, which are difficult or impossible to control during the operation. For optimal functioning of the device, its axis should be close to parallel with the septum, facing the mitral valve within the left ventricle. Our aim is to provide an innovative solution for these problems, using 3D technology and 3D printing. In our work, the production of the patented exoskeleton and the validation of its volumetric and surface quality, was presented, by comparing the virtual and 3D printed exoskeletons.

Keywords: cardiac surgery; mechanical circulatory support; 3D technology; 3D printing; personalized medicine

1 Introduction

According to the World Health Organization (WHO), cardiovascular diseases are the leading cause of death worldwide. Among cardiovascular diseases, end-stage heart failure is one of the most severe syndromes, with constantly increasing morbidity- and mortality rates [1]. For patients in end-stage heart failure who are unresponsive to medical treatments, the gold standard therapeutic option is transplantation. However, the access to donor candidates for heart transplantation is limited [2] [3]. The implantation of a left ventricle assist device (LVAD), is a life-saving treatment option for these patients [4]. A LVAD is a mechanical pump with an external battery, that helps pumping blood from the left ventricle (LV) to the systemic circulation, thereby capable of partially or completely replacing the function of a failing heart [5].

Figure 1 shows the four main parts of the LVAD: the **pump**, the **inflow cannula**, the **outflow cannula** and the **driveline**. For further information about the device structure and function, see the paper of Englert et al. [6], and the paper of Worku et al. [7].

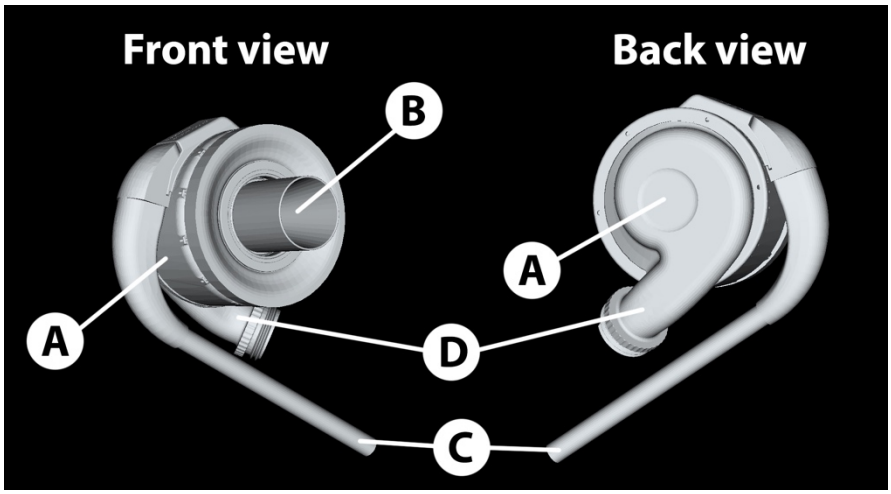

Figure 1
Virtual 3D model of the left ventricle assist device. A: Pump, B: Inflow cannula, C: Driveline, D: Outflow cannula

Success of the LVAD implantation largely depends on the position of the device, however ideal positioning is determined by various factors, that cannot be or are difficult to influence [8] [9]. Ideally, the inflow-cannula (IC) of the LVAD should be parallel with the interventricular septum (IVS) and should point towards the center of the mitral valve (MV). Based on literature data, the ideal degree between the IC and the IVS should be within -7 and +7 degrees of the left ventricular septal

axis [8], otherwise the unfavorable postoperative fluid mechanics of the left ventricle may lead to life-threatening events [10]. Directly after implantation, one of the most severe complications is the suction event, when the pump draws the IVS to the IC, causing the LVAD to stop immediately [11].

The computational fluid dynamical simulation (CFD) is becoming a more and more prominently used mechanical engineering tool in the field of medicine. Using CFD, cardiovascular experts could gain a better knowledge of blood flow dynamics in the left ventricle around the IC. The CFD provides an opportunity for simulation before the clinical usage of new medical devices, facilitating the development of new medical interventions. Despite the CFD simulation advantages, the limitation must be considered [12].

In the field of dentistry and oral surgery, static prefabricated surgical guides are utilized to execute the navigated positioning of dental implants [13] [14]. Dentists and oral surgeons utilize 3D data acquired from cranio-facial computed tomography (CT) scans to determine implant positions and to manufacture surgical guides [15]. Similarly, routine presurgical computed tomography angiography (CTA) scans can be utilized to digitally plan LVAD positions and perform a navigated surgical treatment.

Hence, the aim of this article was to describe a computer-aided design and computer-aided manufacturing process to produce a surgical positioning tool (exoskeleton) for LVADs and to validate the accuracy of the additive manufacturing procedure. The exoskeleton is under the process of international patent protection [16].

2 Materials and Methods

2.1 Image Acquisition

Prior to surgery, spiral electrocardiogram (ECG)-gated thoracic CTA scans are acquired utilizing a multidetector CT machine. Angiographic contrast imaging lasts for one cardiac cycle, during which the machine is capable to take multiple images. 3D planning is carried out relying on images taken at the end-diastolic stage.

Iodine-based intravenous contrast materials are utilized to enhance the visibility of the vessels during radiographic imaging. At the end-diastolic phase, the contrast agent clearly draws out the inner surface and the inner structures of the left ventricle. Therefore, the IVS, the MV, the mitral annulus, and the papillary muscles can be separated from each other. During the virtual model building process, these structures can be reconstructed in 3D. The given flowchart below illustrates our study structure (Figure 2).

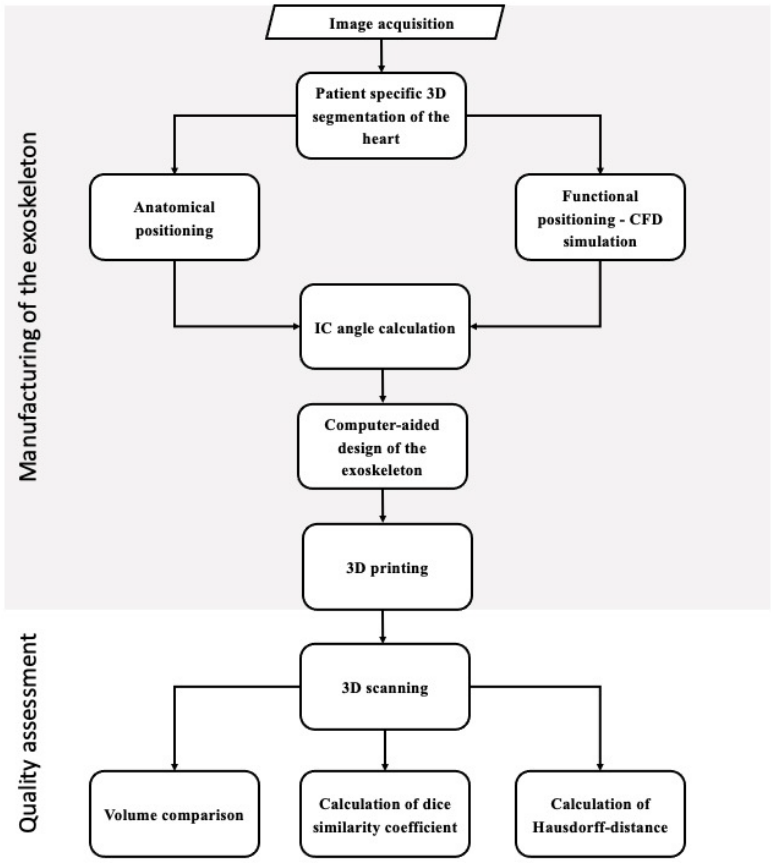

Figure 2
The flowchart illustrates the steps of the exoskeleton manufacturing and quality assessment process

2.2 Radiographic Image Segmentation

DICOM (Digital Imaging and Communications in Medicine) datasets were imported into an open-source medical image processing software (3D Slicer v5.4.0, Boston, MA, USA) [17]. During image segmentation, a binary labelmap for every corresponding anatomic structure is being generated on the multiplanar CTA images (Figure 3). Semi-automatic external heart surface segmentation consists of the following steps: (i) edge detection: outlining the borders of the heart on 5-7 axial slices of the CTA dataset, utilizing a voxel intensity level tracing tool; (ii) morphological contour interpolation: based on the outline of the previously

generated labelmaps, the algorithm calculates the labelmaps on interim slices, interpolating between slices drawn by free hand; (iii) Gaussian method is utilized to smoothen the outline of the binary labelmap. Labelmaps for the internal anatomic structures of the left ventricle (i.e., IVS, MV, papillary muscles) are generated within the area of the previously created labelmap of the heart. Local thresholding segmentation is applied to generate a labelmap for the cavity of the left ventricle. After occasional manual correction and smoothing, the labelmap representing the cavity of the left ventricle is subtracted from the labelmap representing the entire heart. All steps of the segmentation were inspected by a radiologist, a cardiologist and a cardiac surgeon. If necessary, the model was changed with the full agreement of the clinical specialist.

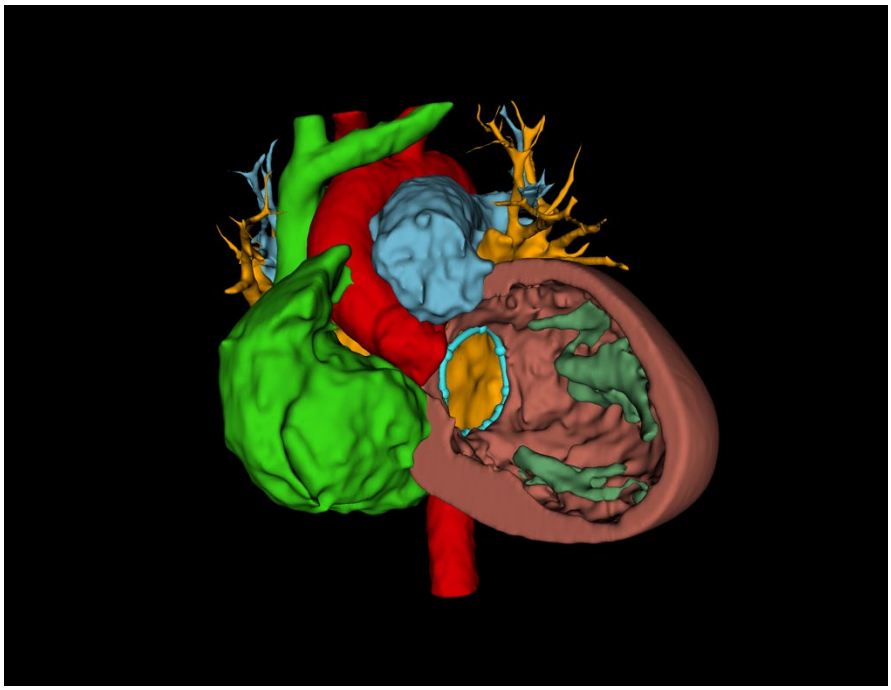

Figure 3

3D model of the segmented heart. A patient-specific computational model provides the possibility to design a personalized exoskeleton for the LVAD implantation. Neon green: right atrium, red: aorta, blue: pulmonary artery, orange: left atrium, brown: heart muscle (myocardium), green: papillary muscles, blue circle: mitral annulus.

With real-time rendering, the software automatically generates a 3D surface representation of the 2D binary label map. 3D surface representation of the segmentation is exported as a Standard Tessellation Language (STL) file.

2.3 Positioning of the IC

2.3.1 Anatomic Positioning

A 3D model of the segmented heart (with the inner structure of the left ventricle), and the 3D model of the LVAD are imported into the Autodesk Fusion 360 (**AutoDesk** Inc. San Rafael, CA, USA) 3D CAD software for the anatomical positioning of the device (Figure 4). The LVAD is placed (i) at 5-15 mm distance from the IVS, (ii) at equal distance from the papillary muscles and (iii) the IC should point towards the center of the MV. The final result of the anatomical positioning step is to orient the LVAD and inflow cannula inside the left ventricle.

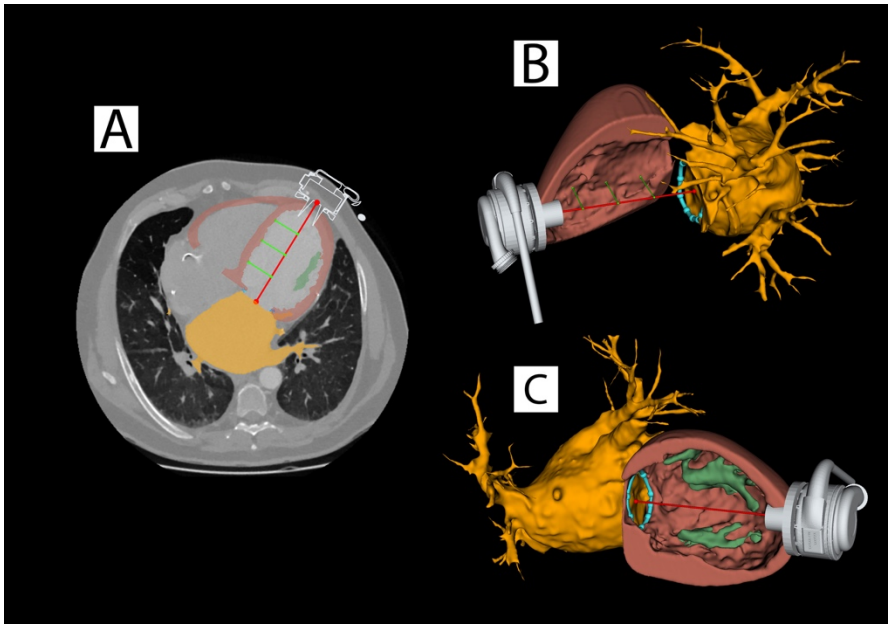

Figure 4

Anatomic positioning of the LVAD **A:** the axial plane of the CT angiography shows the distance (neon green lines) between the inflow cannula's axis (red line) and the interventricular septum (current distance: 13.2 mm); **B-C:** the relation of the IC long axis with the papillary muscles (green) and the mitral annulus (blue circle)

2.3.2 Functional Positioning – Computational Fluid Dynamic Simulation

During the functional positioning step, the most preferable angle was calculated, using CFD simulation, Ansys Fluent 2022 R1 (**ANSYS** Inc. Southpointe, Canonsburg, PA, USA). In our model the left ventricle geometry was patient specific, but other CFD factor was standardized. For fine-tune the IC position for

ideal postoperative ventricular blood flow, a CFD simulation is carried out for all 5 different potential IC angles. A pivot point is placed at the intersection between the IC long axis and the heart muscle, where the LVAD will be implanted. The IC is then rotated into 5 different angles: the center and the four corner points of the MV. Subsequently, fluid mechanical analysis is performed for all 5 potential IC angles.

Standardized fluid characteristics of blood are programmed into the CFD simulation software. Our fluid simulation based on the research of Chivukula et al. [8], and Méndez et al. [18] theoretical flow simulation setup. During the simulation thrombus formation factors were not conducted. Blood is treated as a non-Newtonian fluid with a viscosity of 3.5 mPa·s and a density of 1050 kg/m^3. The inlet part of the heart was the mitral valve, and the inlet boundary condition was specified in flow velocity as 180 m/s, with no pulsatility. Meanwhile, the outlet boundary condition is set on top of the IC inside the left ventricle, with the same conditions as at the inlet point. The inner diameter of the IC was measured as 23.5 mm, while the outer diameter was 25 mm, maintaining a 1:1 ratio with the original device. The insertion depth of the IC was calculated as the difference between the original length of the IC (22 mm) and the thickness of the left ventricle (7.2 mm ± 2.1 mm). The wall (heart muscle) boundary condition is defined as no-slip condition, wherein the normal component of velocity is fixed at zero, and the tangential component is set equal to the velocity of the wall.

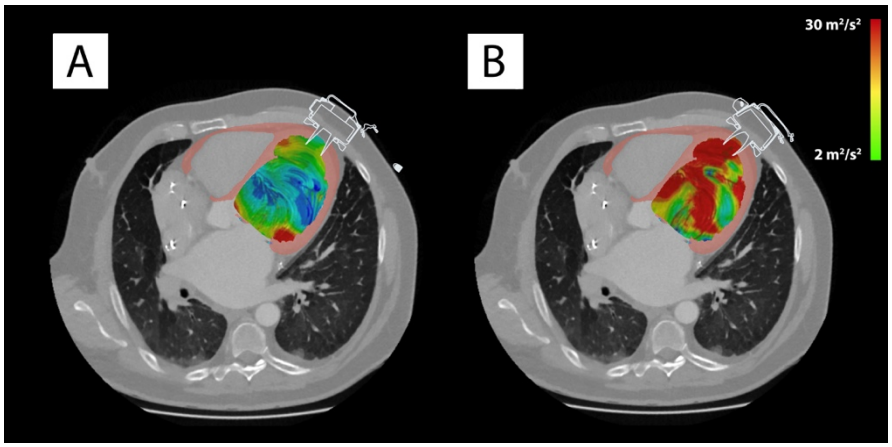

Figure 5

Functional positioning of IC based on CFD simulation. The colormap reveals the turbulence differences between the proper and malpositioned LVAD flow patterns. **A:** turbulence in case of optimal angulation; **B:** turbulence in case of malpositioned IC inside the left ventricle.

During CFD simulation, fluid inflow is set to the MV, whereas fluid outflow is set to the IC of the LVAD. For each of the 5 possible IC positions, turbulence is calculated. Colormap visualizes turbulence values, expressed as: m^2/s^2; the ideal turbulence value for the LV should be between 2 m^2/s^2 and 22 m^2/s^2. The angle with

the most ideal blood flow dynamic is selected as the final planned position of the LVAD (Figure 5).

2.4 Computer-aided Design of the Exoskeleton

The exoskeleton is designed in the Autodesk Fusion 360 (**AutoDesk** Inc., San Rafael, CA, USA) 3D CAD software, capable of free-form surface modelling (Figure 6). The base of the exoskeleton is designed over the outer surface at the apex of the heart, utilizing the heart model generated with the segmentation of the CTA scans. The convex surface of the exoskeleton provides an appropriate fit on the outer surface of the patient's heart during the operation. The extent of the exoskeleton is limited as much as possible, to allow for a minimally invasive incision design and surgical wound, while still providing sufficient support for the guidance of the coring knife. The coring knife is a specific surgical instrument, that is used to cut out a cylindrical shape of the heart muscle for the implantation of the inflow cannula. The guide base spans from the apex of the heart to the IVS with a final leaf-like shape.

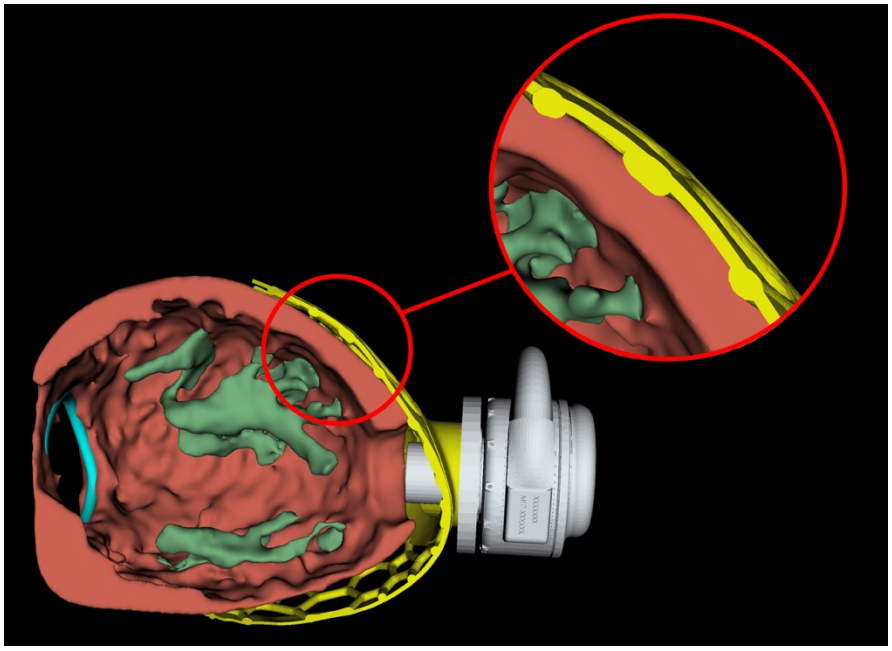

Figure 6
The exoskeleton fits precisely on the surface of the heart. Precise fitting ensures the proper positioning of the IC during the surgical implantation.

At the final position of the IC, a cylindrical guide channel (guiding tube) with a diameter that is capable of housing the coring knife is designed into the exoskeleton base, at the planned anatomical position and preferable angle of the IC. This tube will guide the coring knife during surgery, ensuring that the LVAD will be placed in the planned position. Finally, a Voronoi-pattern is applied to skeletonize the base of the guide, hence the name exoskeleton. The final step of CAD modelling is the smoothing procedure of the exoskeleton. All sharp edges are removed, avoiding any kind of geometry distortion around the guiding tube. At the end of the process, the virtual exoskeleton is suitable for 3D printing and surgical use.

Once the design is finalized, the model of the exoskeleton is exported as a standard tessellation language (STL) file, and is prepared for 3D printing and quality control.

2.5 Additive Manufacturing of the Exoskeleton

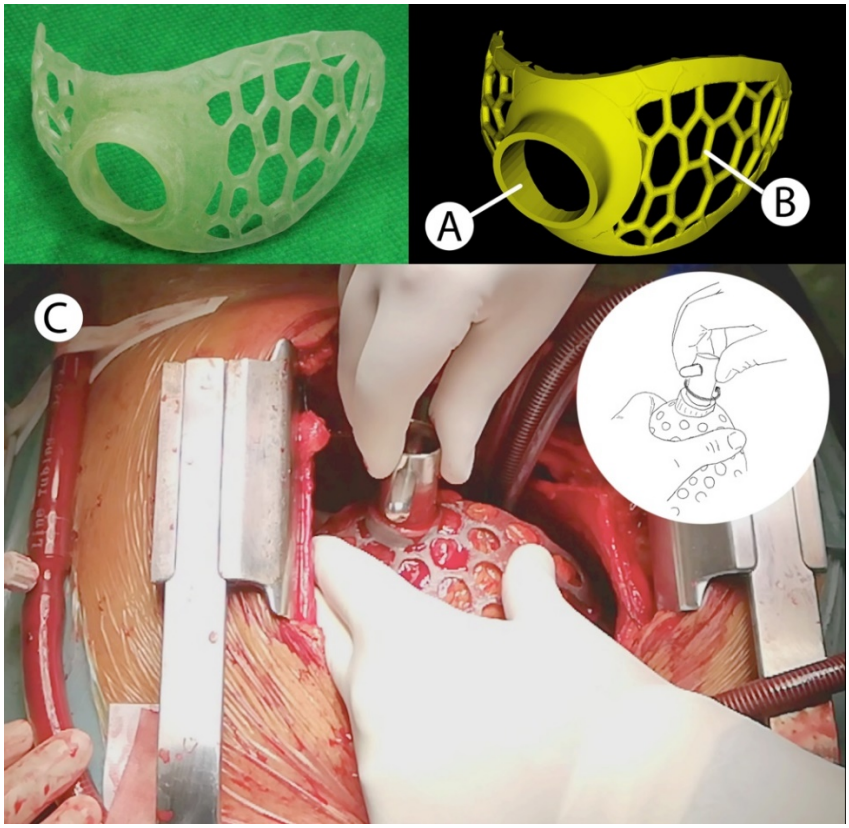

Figure 7
3D digital model, additively manufactured model and surgical implementation of the exoskeleton. **A:** guiding tube for the coring knife, **B:** Voronoi-pattern skirt of the exoskeleton, which ensures a clear view to confirm proper fit of the exoskeleton. **C**: Surgical use of the exoskeleton

The STL file of the exoskeleton is imported to the dedicated software of a 3D printer capable of producing devices suitable for surgical applications. A wide variety of printers are available on the market using stereolithography (SLA) technology, which can be utilized to manufacture the exoskeleton. A sterilizable medical grade photopolymer resin (USP class VI; ISO 10993-5, -10, -23) with adequate mechanical properties can be utilized to manufacture the exoskeleton (Figure 7). Prior to surgery, the exoskeleton is sterilized in an autoclave at 121 °C for 30 minutes [19].

2.6 Outcome Measures - Quality Control of the Printed Exoskeleton

Fifteen patient-specific virtual 3D exoskeleton (VE) masks were extracted, accompanied by the retrieval of their corresponding 3D printed exoskeleton (3DPE) models. The 3D scanning process was carried out using a desktop optical 3D scanner (Einscan-SP V2, SHINING 3D, Hangzhou, China), which ensured high-resolution point cloud data with an exceptional single-shot accuracy of 0.05 mm, conforming to the ISO 12836 standard. These data were then transformed from 'Mask to Surface' utilizing a 3D inspection software, Geomagic Control X (3D Systems, Rock Hill, SC, USA). Later it was used to generate colormaps between the VE STL file, and the re-scanned 3DPE, STL file (Figure 8).

The two datasets (from VE and 3DPE) were registered. The VE was chosen as the fixed reference dataset and the corresponding printed model surface for the corresponding registration dataset. To ensure uniformity, six consistent anatomical landmarks were manually pinpointed on each surface. This selection comprised three landmarks on the convex surface and an additional three on the concave surface, situated within the upper, middle, and lower regions of both the VE and 3DPE surfaces.

The VEs were compared to the 3DPE scans, to validate the accuracy of the manufacturing process. The primary outcome measure was the volumetric difference between the VE models and the 3DPE models.

Secondary outcome measures were: dice similarity coefficient (DSC) and Hausdorff-distance (HD). These metrics assessed the surface quality between the VE and 3DPE models. The DSC uses a reproducibility validation metric and an index of spatial overlap. DSC values range from 0 to 1, which denotes the entire spatial similarity between the two objects. The value of 1 means a total overlap between two 3D models [20].

On the other hand, the Hausdorff-distance [21] measures distance between two-point sets. Thus, this distance can be used to determine the degree of resemblance between two objects that are superimposed on one another. Three different values were measured on the models: (i) maximum, (ii) average distance between two points, and (iii) the 95^{th} percentile of measured distances.

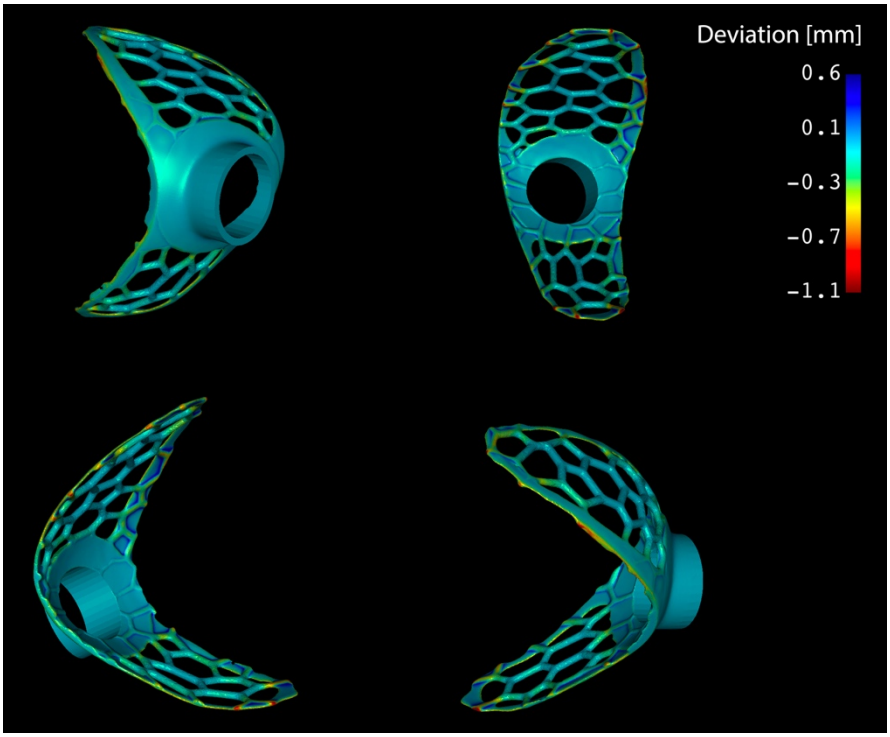

Figure 8
Comparison of the VE and 3DPE models. The surface similarity data were visualized in a deviation map, where the colors red, orange and yellow describe areas with negative material discrepancy, while cyan and blue colors describe areas with surplus material compared to the original STL object.

In all cases, the master and scanned models were considered identical, if the DSC was greater than 0.9 and the HD 95th percentile was less than 1mm.

Statistical significance between the values of each outcome measure was calculated paired t-test with a significance level of 0.05. Statistical evaluation was done with SPSS Statistics (IBM, Armonk, NY, USA).

3 Results

3.1 Primary Outcome – Volumetric Differences

The volume comparison between the VE model and the 3DPE model revealed no statistically significant difference (p= 0.76). Volume of the VE models averaged at

10.81 cm^3 ± 1.69 cm^3, whereas average volume of the 3DPE models were 10.80 cm^3 ± 1.70 cm^3. Volumetric differences are shown in Figure 9.

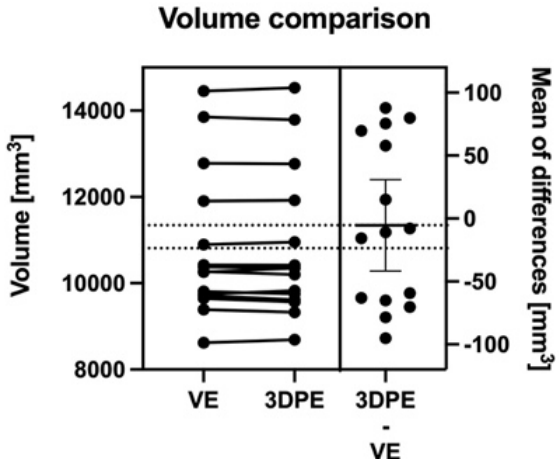

Figure 9
Estimation plot of the virtual exoskeleton (VE) and 3D printed exoskeleton (3DPE).

3.2 Secondary Outcome Measures – Surface and Volumetric Quality Assessment

The surface quality measurements did not show considerable differences. Spatial overlap between the VE and 3DPE models measured by the DSC showed an average 0.95 ± 0.03 value (minimum: 0.91, maximum: 0.98). The maximum HD value averaged at 2.83 mm ± 1.31 mm. Whereas, the mean HD distance between VE and 3DPE averaged at 2.17 mm ± 0.52 mm, with an average 0.16 mm ± 0.06 mm 95th percentile HD value. The 95th percentile of the distance was less than 1mm in every scanned exoskeleton. DSC and HD values are shown in Table 1.

Table 1
Surface quality measurements of the virtual and the 3D printed exoskeleton.

	Dice similarity coefficient	**Hausdorff-distance**		
		Maximum [mm]	**Average [mm]**	**95% [mm]**
Maximum	0.98	2.83	0.26	0.94
Minimum	0.91	1.31	0.08	0.31
Mean	0.95	2.17	0.16	0.60
SD	0.03	0.52	0.06	0.21

4 Discussion

The aim of the current paper was to describe the fundamental aspects of planning a navigated surgical LVAD implantation, and the additive manufacturing of the patented exoskeleton. Re-scanning of the actual 3D printed exoskeletons provides an ideal solution to compare the volume- and the surface stability of two 3D models.

The implantation of an LVAD is a highly technical, sensitive procedure, that mostly relies on previous LVAD implantation experience. Therefore, it is implemented in expert and high-volume centers, as these are associated with a low risk of post-operative bleeding, infection, RV failure and mortality [22]. Yet, even in the hands of an experienced surgeon, results may differ greatly, without the navigated placement of the device. Unfavorable postoperative IC position, caused by inadequate implantation, has negative consequences. The malposition of the device may increase the risk of postoperative complications on long term [10]. The incidence of the complications mentioned in section introduction, arising from device misplacement, could potentially be diminished or entirely prevented through the implementation of the exoskeleton. Important to note that this study did not gather data on long-term postoperative complications. Therefore, additional research is required to prove our device positive effects on clinical outcomes.

A case report demonstrating the clinical application of the intra-surgical application of the exoskeleton has previously been published by our group [19]. In that case, the accuracy of the LVAD position was validated by comparing angulations between the IVS and the IC on the preoperative plan and the postoperative control CT scan. The deviation between the planned position and the actual postoperative position of the IC was 2.6°. In a recently published article by Pearman et al., the authors demonstrated an average of 16.3°–23.2° deviation between the actual IC position and the postoperatively determined hypothetical ideal IC position (the axis connecting the center of the MV and the center of the IC) [23]. Although slightly different reference axes were utilized in the two studies, and it is difficult to compare one single case to a series of 42 cases, the difference in deviation from the ideal values is remarkable. Based on our clinical experience, and so far, unpublished data, high accuracy surgical results can be achieved with high reproducibility. Additionally, with the application of the exoskeleton, postoperative outcomes seem to be influenced less by the experience of the surgeon. An additional benefit of 3D virtual planning is that the surgeon has a more accurate insight of the patient's anatomy. Besides planning, virtual and/or 3D printed anatomical models can be utilized during surgery to visualize anatomical relations of different structures, even in cases with limited direct visualization.

With the re-scanning process it was demonstrated that the 3D printed exoskeleton does not show considerable differences to the original digital model. Only the edges reveal more than 1 mm distance inequality, at a maximum value of 2.83 mm. This occurrence is most likely due to the post-processing of the 3D printed models, namely the removal of the support structure. During the post-process, the edges of the exoskeleton were rounded with a bur. This post-process step is essential to manufacture a safe surgical instrument, which can be used during the operation. On the other hand, the average 95th percentile of two points distance was 0.60 mm, which is noticeably less than the accepted 1mm distance difference. The distance observed on the concave surface of the exoskeleton measures below 0.1 mm (0.04 ± 0.038 mm). The convex surface around the guiding tube determines the accuracy of the implantation process. This indicates that the quality of the exoskeleton was sufficient for surgical application. DSC values marking the spatial overlap between the VE and 3DPE models averaged at 0.95 ± 0.03. Results of the volumetric measurements are in line with the surface assessment, with no statistically significant difference between the volume of the VE and the 3DPE models.

While the medical discipline holds significant promise for the application of CFD simulation, establishing accurate model parameters proves to be a challenging task. This difficulty arises from the fact that the properties of blood undergo changes in varying environments [12] [24]. Consequently, the concept of simulating patient-specific scenarios becomes a topic of discussion in existing literature, particularly when considering essential thrombosis-related parameters such as activated platelets, resting platelets, prothrombin concentration, anti-thrombin III concentration, and other factors. For that reason, standardized parameters were used in our simulation, conducting a theoretical flow simulation.

Because of this limitation, CFD was exclusively utilized to refine the positioning of the inflow cannula. The patient specific anatomy of the left ventricle defined the position of the inflow cannula. The CFD approach was aimed at demonstrating the future capabilities of CFD in effectively determining the optimal positioning of LVADs. Another drawback of the technique is the relatively long duration of the planning process and the fact, that the user must have a complex knowledge, in radiographic image processing, CAD modelling and 3D printing. Some of the steps (e. g., segmentation, CAD modelling of the exoskeleton) still require substantial human interaction. The automation of these processes shall be possible in the future with the development of deep learning segmentation algorithms and dedicated software, to reduce the duration of the planning phase and to reduce the rate of occasional human-made errors.

Conclusions

3D modeling and printing have proven to be promising technologies, with impressive potential applications for medicine. Among other benefits, they provide the possibility to plan surgical procedures, even before the first incision. In our ongoing study, all cases were prepared with the help of a virtual, patient-specific

3D model of their heart, with the surrounding vessels and organs. The overall responses from the operating surgeons to this technology were positive. The main opinion is, that 3D technology supports the success of the surgical intervention. However, the leading barrier for the use of 3D technology in clinical practice, is the accessibility of the necessary engineering knowledge (usage of different software, 3D modeling and printing, post processing and availability of a 3D printer). With the enthusiasm for this technology, comes the need for the standardization of the technique, the establishment of a clinical facility and improved accessibility.

It can be concluded, that, with the elaborative planning process, the LVAD can be implanted into an ideal position. Therefore, the complication rate of IC malpositioning could be reduced or completely avoided. The exoskeleton is a surgical instrument which provides the possibility of a personalized, calculation-based implantation of the LVAD. One of the mayor drawbacks of the current planning process is the lack of a patient specific, thrombus formation simulation. Therefore, in the future, individualized haemostaseology processes will be considered, during the planning stage. In order to evaluate the clinical performance of the device, large sample comparative studies must also be conducted.

Acknowledgement

This work was supported by the Semmelweis Science and Innovation Fund as part of the "STIA-KFI-2020" research and development project.

References

[1] Roger, V. L. et al.: Epidemiology of Heart Failure: A Contemporary Perspective, Circulation research, 2021, Vol. 128, pp. 1421-1434

[2] Tatum, R. et al.: Evaluation of donor heart for transplantation, Heart failure reviews, 2022, Vol. 27, pp. 1819-1827

[3] Severino, P. et al.: Advanced Heart Failure and End-Stage Heart Failure: Does a Difference Exist, Diagnostics (Basel, Switzerland), 2019, Vol. 170, pp. 65-71

[4] Varshney, A. S. et al.: Trends and Outcomes of Left Ventricular Assist Device Therapy: JACC Focus Seminar, Journal of the American College of Cardiology, 2022, Vol. 79, pp. 1092-1107

[5] Pietras, C. et al.: Surgical Implantation of Intracorporeal Devices: Perspective and Techniques, Cardiology clinics, 2018, Vol. 36, pp. 465-472

[6] Englert, J. A. R. et al.: Mechanical Circulatory Support for the Failing Heart: Continuous-Flow Left Ventricular Assist Devices, The Ochsner journal, 2016, Vol. 16, pp. 263-9

[7] Worku, B. et al.: Thoracotomy versus sternotomy? The effect of surgical approach on outcomes after left ventricular assist device implantation: A review of the literature and meta-analysis, J Card Surg, 2021, Vol. 7, pp. 2314-2328

[8] Chivukula, V. K. et al.: Left Ventricular Assist Device Inflow Cannula Angle and Thrombosis Risk, Circulation Heart failure, 2018, Vol. 11, pp. 23-41

[9] Chivukula, V. K. et al.: Small Left Ventricular Size Is an Independent Risk Factor for Ventricular Assist Device Thrombosis, ASAIO journal (American Society for Artificial Internal Organs: 1992), 2019, Vol. 65, pp. 152-159

[10] Schlöglhofer, T. et al.: Inflow cannula position as risk factor for stroke in patients with HeartMate 3 left ventricular assist devices, Artificial organs, 2022, Vol. 46, pp. 1149-1157

[11] Kortekaas, K. A. et al.: Left ventricular assist device and pump thrombosis: the importance of the inflow cannula position, The international journal of cardiovascular imaging, 2022, Vol. 38, pp. 2771-2779

[12] Lee, B. K.: Computational fluid dynamics in cardiovascular disease, Korean circulation journal, 2011, Vol. 41, pp. 423-430

[13] Ganz, S. D.: Three-dimensional imaging and guided surgery for dental implants, Dental clinics of North America, 2015, Vol. 59, pp. 265-290

[14] Sass, T. et al.: Esthetic and functional reconstruction of large mandibular defects using free fibula flap and implant-retained prosthetics - a case series with long-term follow-up, Head & face medicine, 2021, Vol. 17, p. 43

[15] Palkovics, D. et al.: Digital Hybrid Model Preparation for Virtual Planning of Reconstructive Dentoalveolar Surgical Procedures, Journal of visualized experiments: JoVE, 2021, Vol. 174, pp. 16-25

[16] Barabás, I. J. et al.: Exoskeleton for assisting surgical positioning, method for producing the exoskeleton and a surgical method applying such an exoskeleton, Patent, 2018, PCT/HU2019/050049

[17] Herz, C. et al.: dcmqi: An OpenSource Library for Standardized Communication of Quantitative Image Analysis Results Using DICOM, Cancer research, 2017, Vol. 77, pp. 87-90

[18] Méndez R. R. et al.: Multi-constituent simulation of thrombus formation at LVAD inlet cannula connection: Importance of Virchow's triad, Artificial organs, 2021, Vol 45, pp. 1014-1023

[19] Barabás, I. J. et al.: A 3D printed exoskeleton facilitates HeartMate III inflow cannula position, Interactive cardiovascular and thoracic surgery, 2019, Vol. 29, pp. 644-646

[20] Krithika Alias AnbuDevi, M. and Suganthi, K.: Review of Semantic Segmentation of Medical Images Using Modified Architectures of UNET, Diagnostics (Basel, Switzerland), 2022, Vol. 12, p. 3064

[21] Taha, A. A. and Allan H.: Metrics for evaluating 3D medical image segmentation: analysis, selection, and tool, BMC medical imaging, 2015, Vol. 15, p. 12

[22] Loforte, A. et al.: Ventricular assist devices implantation: surgical assessment and technical strategies, Cardiovascular diagnosis and therapy, 2021, Vol. 11, pp. 277-291

[23] Pearman, M. et al.: Comparing left ventricular assist device inflow cannula angle between median sternotomy and thoracotomy using 3D reconstructions, Artificial organs, 2022, Vol. 29 p. 144

[24] Berg, P. et al.: A review on the reliability of hemodynamic modeling in intracranial aneurysms: why computational fluid dynamics alone cannot solve the equation, Neurosurg Focus, 2019, Vol. 47 p. 15